Regimes of falling liquid film flowing over the vertical cylinder at contact angles up to 90° and Reynold number 50

Alexey Sakhnov*, *Oleg* Volodin, *Nikolay* Pecherkin, and *Alexandr* Pavlenko

Kutateladze Institute of Thermophysics SB RAS, 630090 Lavrentyiev Ave. 1, Novosibirsk, Russian Federation

Abstract. The paper presents 3D numerical modeling of spreading dynamics of R21 (mol. fraction: 0.9) and R114 refrigerant mixture film. We considered an outer flow along a round vertical cylinder at Reynolds numbers of 50 and contact angles of 10°, 30°, 50°, 70° and 90°. The simulation was performed in OpenFOAM software on the basis of the volume of fluid (VOF) method. We obtained that the contact angle has a key effect on the wetted area due to the change of liquid spreading modes over the cylinder. At that, we distinguished the following flow modes: the stable jet mode, the cascade jet mode, the jet-droplet mode and the drying mode. These modes are similar ones for horizontal tubes. In some flow modes over the vertical cylinder, we demonstrated the existence of the back liquid flow between jets, directed against gravity.

1 Introduction

Falling films are widely used in various technical devices to enhance heat and mass transfer. Dai et al. [1] did a review of works on heat exchangers in desalination systems, where a character of film spreading plays a main role in processes of heat and mass transfer. Authors distinguished three main types of falling-film evaporators with horizontal or vertical tubes and vertical plates. Following paper [2], Dai et al. defined six flow modes of a liquid film falling on horizontal tubes in the range of film Reynolds number $Re = 2\Gamma/\mu = 1.3 - 64$. With the increase of Reynolds number, the flow mode of liquid transforms from the droplet mode through various jet modes to the sheet mode. In work [3] authors demonstrated that the counter flow of the gas phase changes Reynolds numbers for these flow modes. The above-mentioned works do not take into account a relation between the film flow mode and wetting angle.

Using OpenFOAM software, Karmakar and Acharya [4] numerically modelled film flow of water and ethylene glycol mixture over the horizontal tubes with fully wetted surface ($\theta = 0°$) at $Re = 2\Gamma/\mu = 15$ - 210. The authors obtained detailed characteristics of the above-mentioned film flow modes and confirmed the effect of Reynolds number on the transition from one mode to another.

Ramadan and Park [5] performed a simulation of the water falling film over horizontal tubes at $Re = 4\Gamma/\nu = 12$ and $\theta = 0°, 30°, 60°$ using the VOF-method. The authors modeled Reynolds numbers of 12, 24 and 36 for the contact angle of 10°. In work [6] Arroiabe et al. investigated LiBr-H2O flow over the horizontal tubes in wider ranges of Reynolds number ($7 < Re < 53$) and contact angle ($0° < \theta < 120°$). Both works showed that the increase of the contact angle transforms the character of the film flow from the jet mode to the droplet one at a fixed Reynolds number. The effect of Reynolds number on the film flow mode correlates with the results of work [2].

Iso and Chen [7] and Sebastia-Saez et al. [8] simulated by VOF-method a liquid film flow falling over the inclined plate with smooth or structured surfaces. In both works, the authors use Weber number $We = \rho V^2\delta/\sigma$ to classify the film flow mode. For the smooth surface with $\theta = 70°$, the droplet mode takes place at Weber numbers of 0.03 [8] and 0.04 [7], the jet mode does at Weber numbers of 0.42 [7], 0.8 [7, 8] and 1.14 [7], and the liquid film covers uniformly the whole considered surface at $We = 1.4$ [8] and $We = 1.44$ [7]. Taking into account the relation $We = Re\mu V/\sigma$ and the fixed contact angle, the results of the simulation correspond to the conclusions of paper [2] on the effect of Reynolds number on the film flow mode for horizontal tubes. In paper [9] authors demonstrated that the decrease of the contact angle increases an area of interface.

In work [10] Sebastia-Saez et al. numerically studied the effect of contact angle on the rivulet characteristics at $\theta = 20°, 23°, 24°, 34°, 60°, 100°$. The authors demonstrated that there is a minimum at $\theta = 60°$ in the dependencies of the width and contour lengths of rivulets. However, since flow cases at $60° < \theta < 100°$ were not investigated, then minimums of these characteristics may exist within the pointed range of the contact angle. The interface area decreases with the increase of the contact angle, including solvophobic flow case.

* Corresponding author: sakhnov@itp.nsc.ru

Lavalle et al. [11] simulated water/glycerin (50% and 80%) film flow over the vertical plate without sidewalls at $Re = V_0\delta/\nu = 1.2 – 101$ and $\theta = 40° – 160°$. The authors demonstrated a cascade character of the rivulets occurrence under such conditions. Due to the absence of the sidewalls first rivulets arise on the left and right borders of the spreading film. If the film has enough width, then at further flow the second and the third couples of rivulets take place on the same distance from the first couple. Modelling of the water/glycerin (80%) film at $Re = 2.92$ showed that the contact angle increase has no effect on the cascade character of the occurrence of rivulets and on its number, but it increases the length of rivulets.

In work [12] Ishikawa et al. studied water and methanol film flows over the micro-baffled plate. The authors demonstrated that liquid film parameters coincide with each other for flows with contact angles of 10°, 30° and 60°. In other words, baffles, placed at a certain distance from each other, redistribute the liquid in horizontal direction preventing film break.

Haroun et al. [13] numerically modeled liquid film flows at $\theta = 10°, 30°, 70°$ and $Re = 4\rho l V_0\delta/\mu l = 220, 344, 800$ in structured packings. The authors showed that the liquid forms rivulets at the maximal contact angle and the minimal Reynolds number while it fully covers the surface of the structured packing at the highest Reynolds number and the lowest contact angle.

Gu et al. [14] performed numerical research on the flows of liquid oxygen and water in structured packing at $\theta = 0.1°, 5°, 10°, 30°, 70°$ and $We = 4\rho v^2\delta/\sigma = 0.29 – 9.98$. Authors noted that water wets the packing surface better than liquid oxygen at the same contact angle and close Weber numbers of 1.59 (water) and 1.83 (oxygen). It means that the Weber number and contact angle are not able to determine the liquid film flow mode definitely.

Smolka and SeGall [15] experimentally and numerically investigated an outer film flow of silicone oil and glycerin over the vertical cylinder. Cylinder radius varied from 0.159 cm to 3.81 cm. Unfortunately, authors say nothing about the contact angle value. Glycerin did not form practically a continuous film, and liquid fingers take place on the cylinder. Silicone oil kept the continuous film initially with the further occurrence of the liquid fingers. At that, glycerin fingers had clearer contours, and its velocity was higher than the velocity of silicone oil fingers. In addition, the front velocity of the silicone oil between fingers had the lowest value in the flow.

Mayo et al. [16] numerically studied an effect of dimensionless radius on the film flow on the basis of work [15]. The dimensionless radius is calculated by the following formula:

$$\hat{R} = R\left(\frac{\rho g}{\sigma H}\right)^{1/3}, \quad (1)$$

where H is the film thickness. The authors demonstrated that the variation of the film thickness on the cylinder at $\hat{R} = 0.64, 0.72, 0.8$ differs significantly from the film thickness on the vertical plate, while film thicknesses of these flows coincide with each other at $\hat{R} = 1.28$. The similar rivulets exist in both flows with the increase of the dimensionless radius up to 2.56. So, the effect of surface curvature on the film flow is negligible at $\hat{R} > 2.56$, and the number of fingers increases with increase of cylinder radius. Research [17] confirmed these conclusions. Also, Mayo et al. [16] states that the stable continuous film mode takes place on cylinders with $\hat{R} < 0.96$.

Li et al. [18] studied flow characteristics of a liquid film flowing over a smooth vertical cylinder and vertical cylinder with transverse ribbing. The Reynolds number ranged from 10 to 1121. The binary mixture of R21 and R114 refrigerants is used as the working liquid. To capture the liquid film's flow dynamic characteristics and spatial distribution 3D simulations were carried out. It was shown that surface tension has a great influence on the flow pattern, while inlet width has no effect on the film flow parameters at the steady-state flow regime. For both the smooth surface and the ribbed one, flow rates have great effects on wettability, film velocity and film thickness. The simulation also showed that a ribbed surface structure hinders the liquid film movement, reflected in a lower velocity and a larger film thickness compared to the smooth surface. Lateral movement of a film can also be observed at the ribbed surface.

The contact angle has a significant effect on the film flow mode and, as a consequence, on the wetted area and wetting rate. Paper [19] presents results of experimental studies on the film flow dynamics of liquid nitrogen over the complex surfaces: vertical plane and ribbed aluminium plates with/without wave microtexture and perforation. It is shown that the film flow character depends significantly on the wetting rate. The orientation and parameters of microstructure, the angle of corrugation, position and diameter of perforation effect significantly the character of liquid spreading over the surface of the corrugated plates with structure's characteristics typical of those used in Sulzer structured packings [20], especially, within the range of low liquid flow rates.

The above considered works present primarily results on the wetting area and data on the volume phase fraction coefficient α. Our paper includes new film flow data in the form of liquid velocity fields, which allow evaluating both wetting dynamics and local characteristics of the liquid film flow. On the basis of these data, obtained from 3D numerical modelling of the two-phase film flow, we will show the effect of contact angle on the film flow of R21 (mol. fraction: 0.9) and R114 refrigerants over the smooth vertical cylinder at Reynolds number of 50. In order to exclude the evaporation effect on the film spreading, we applied isothermal conditions on the present stage of our research.

2 Flow configuration and modelling approach

We considered the liquid film spreading of the R21 (mol. fraction: 0.9) and R114 refrigerant mixture over the quarter of the round vertical cylinder with a radius of 25 mm and height of 90 mm (Figure 1). The

modelling volume was limited by the imaginary outer cylinder with a radius of 26 – 30.25 mm depending on wetting angle. An area with the initial liquid film thickness δ = 0.25 mm and initial liquid velocity V_0 = -0.048 m/s was set on the upper horizontal plane. Taking into account the properties of the above pointed refrigerant mixture (Tab.1), Reynolds number $\mathrm{Re} = \Gamma/\nu = V_0\,\delta/\nu$ had value of 50 and Weber number ($\mathrm{We} = \rho V_0^2\,\delta/\sigma$) was equaled 0.047 respectively (here Γ is the liquid flow rate per unit of film width, m²/s; ν is the kinematic viscosity m²/s). Kapitza number $Ka = \sigma_l(\rho_l/\mu_l^4\,g)^{1/3}$ had the value of 3801 for all flow cases. The dimensionless radius of the cylinder $\hat{R} = 36.9$ calculated by formula (1) is significantly higher than the critical values, at which the curvature of the cylinder will not have any influence on the film flow.

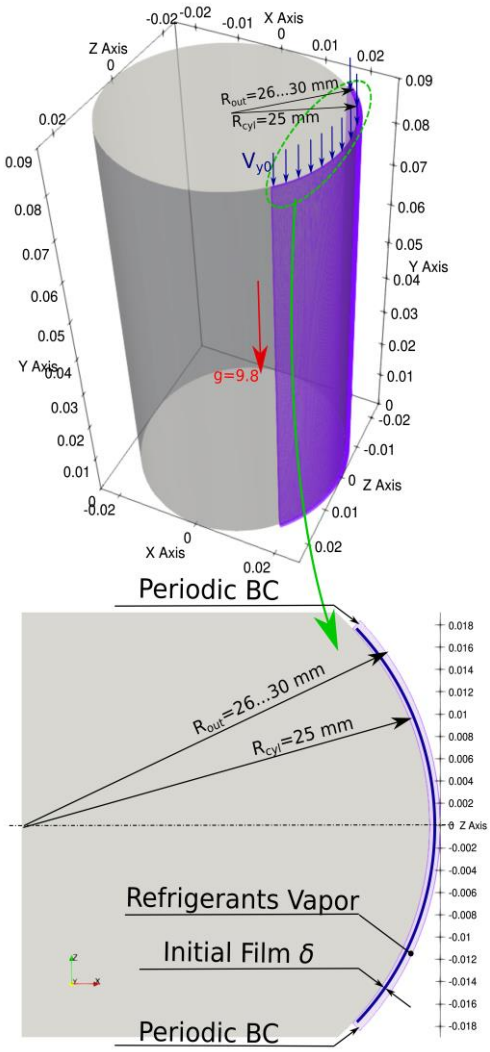

Fig. 1. Diagram of the flow considered.

Table 1. Properties of the R21 (mol. fraction: 0.9) and R114 refrigerant mixture at P = 0.2 MPa and T = 24.94°C.

Properties	Liquid phase
Molar weight, kg/kgmole	109.72
ρ, kg/m³	1379.19
μ, kg/(m·s)	3.32×10^{-4}
σ, N/m	1.68×10^{-2}
c_v, J/(kg·K)	718
Pr	3.4

2.1 Equations and boundary conditions

The simulation was performed in OpenFOAM software on the basis of the volume of fluids (VOF) method [21]. We used solver «interFoam» that consists of the conservation laws of mass and momentum as well as a transport equation for the liquid volume fraction:

$$\frac{\partial\rho}{\partial t} + \nabla\cdot(\rho \mathrm{U}) = 0, \tag{2}$$

$$\frac{\partial\rho \mathrm{U}}{\partial t} + \nabla\cdot(\rho \mathrm{UU}) - \nabla\cdot(\mu\nabla \mathrm{U}) = \\ = \sigma\kappa\nabla\alpha - \mathrm{g}\cdot\mathrm{x}\nabla\rho - \nabla P_d \tag{3}$$

where U is a velocity vector, σ is the surface tension coefficient, κ is the curvature of the interface, P_d is the dynamic pressure and x is the position vector;

$$\frac{\partial\alpha}{\partial t} + \mathrm{U}\cdot\nabla\alpha + \nabla\cdot \mathrm{U}_c\alpha(1-\alpha) = 0, \tag{4}$$

where α is the volume phase fraction coefficient. Values of α = 1 correspond to mesh cells fully filled with the liquid; at α = 0 a mesh cell contains only gas phase, while intermediate values of this coefficient mean the presence of the interface within a mesh cell.

The interaction between velocity and pressure was established by the PISO (Pressure Implicit with Splitting of Operators) algorithm. Also, we considered the laminar regime for both phases and constant liquid density.

The following conditions were applied at borders of the modelling volume.

1. Initialization of the liquid film:

$$y = 0.09: U = V_0, \alpha = 1, dP/dn = 0. \tag{5}$$

2. The solid surface of the cylinder:

$$x^2 + z^2 = R_{cyl}^2: \mathrm{U} = 0, \alpha = 0, \theta = var, dP/dn = 0. \tag{6}$$

3. Free borders of the modelling volume:

$$x^2 + z^2 = R_{out}^2 \text{and} y = 0: \\ U = 0 \text{ or } \partial U/\partial n = 0, \alpha = 0, P = 2\times10^5 Pa. \tag{7}$$

At the initial time (t = 0), the modelling volume had the following parameters: U = (-0.005,0,0), α = 0, $P = 2\times10^5$ Pa.

The contact angle θ in OpenFOAM is used to calculate the curvature in the cells closest to the walls. The following equation defines a vector n_w normal to the interface:

$$n_w = (\nabla\alpha/|\nabla\alpha|)_w = n_n cos\theta + n_t sin\theta, \tag{8}$$

where n_n and n_t are normal and tangential vectors relatively the solid surface. So, the first term of the right side of equation (3), that is the surface tension force, reads in the near wall cells as $\sigma\kappa\nabla\alpha = \sigma(-\nabla \cdot n_w)\nabla\alpha$.

2.2 Mesh

To perform the simulation with contact angles of 10° and 30° we created a hexahedral mesh within a volume limited by outer radius $R_{out} = 26mm$ and a number of cells 20×500×400 (x×y×z) with compression to the solid surface (Figure 2).

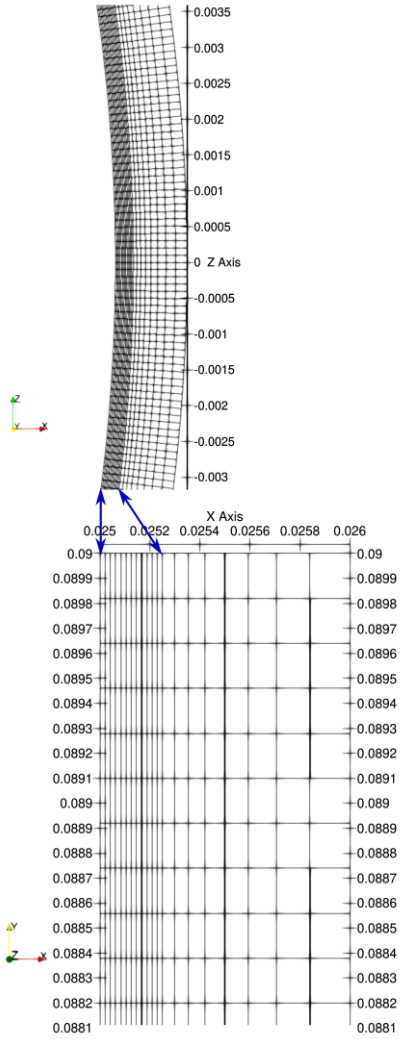

Fig. 2. Parts of meshes in ZX-view (up) and XY-view (down) for film flows at θ = 10°, 30°.

Flows with the higher contact angles of 50, 70 and 90 requested an increased modelling volume with $R_{out} = 30.25\ mm$ and the number of cells 40×500×400 (x×y×z) (Figure 3). The time step did not exceed Δt = 2×10^{-5} s. Both meshes have the following characteristics: maximal aspect ratio – 8.83, minimal cell volume – 3.68×10^{-13} m^3, maximal cell volume – 2.92×10^{-12} m^3 (7.08×10^{-12} m^3), maximal non-orthogonality 3.91×10^{-6}, average non-orthogonality – 0, maximal skewness – 0.0048.

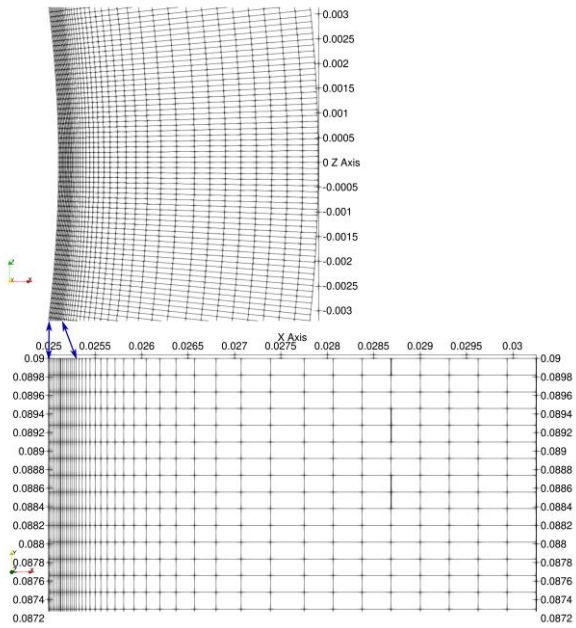

Fig. 3. Parts of meshes in ZX-view (up) and XY-view (down) for film flows at θ = 50°, 70°, 90°.

3 Results

Figure 4 shows the film spreading of the refrigerant mixture over the vertical cylinder at θ = 10°. Short straight jets occur below the continuous liquid film at t = 0.32 s. The jets have the sharp shape of the wetting front. Some disturbances propagate over the continuous film upstream from the wetting front.

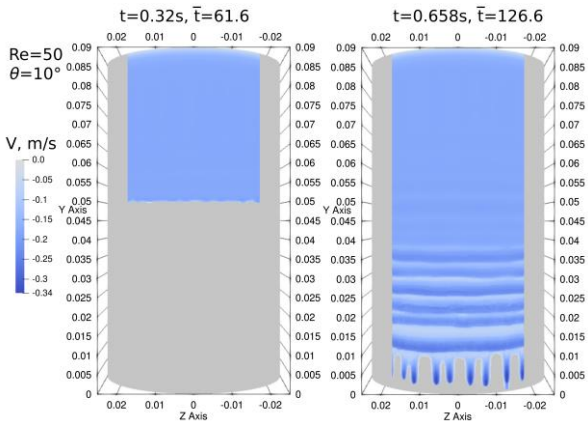

Fig. 4. Fields of the vertical velocity of the liquid (α=0.5) in the refrigerant film flow over the vertical cylinder at θ = 10°.

The local velocity on these disturbances and in jets reaches the maximal absolute value of V = -0.34 m/s that is in 2.5 times higher than the local velocity of the continuous film. The continuous film reaches bottom of the cylinder at t = 0.74 s ($\bar{t} = 142.4$). So, the averaged velocity of the film spreading is 0.121 m/s increasing the initial liquid velocity in 2.5 times.

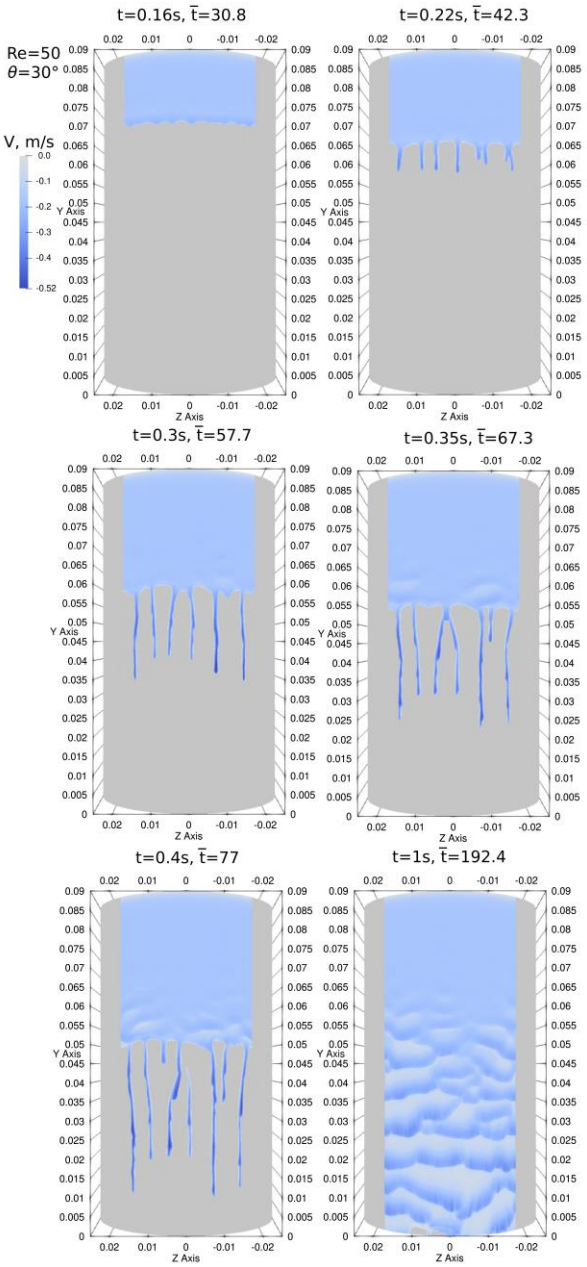

Fig. 5. Fields of the vertical velocity of the liquid (α=0.5) in the refrigerant film flow over the vertical cylinder at $\theta = 30°$.

Figure 5 presents the film spreading of the refrigerant mixture over the vertical cylinder at $\theta = 30°$. Under such conditions irregularities occur on the wetting front rather early at $t = 0.16$ s and at a distance of 17 mm from the upper boundary of the cylinder. To the moment $t = 0.22$ s, the liquid develops short straight jets, which warp and become slightly thinner in further evolution. The jet of the second generation occurs on the right side of the wetting front of the continuous film at t=0.30 s. The merge and disintegration of jets take place since t=0.35 s, and the jet of the third generation develops on the left side of the wetting front of the continuous film at t=0.4 s. So, the liquid film spreading at $\theta = 30°$ has a cascade mode. The film flow mode at $\theta = 30°$ has the following distinctions: the sharp wetting front of the jets, the lower number of the jets in the second and subsequent generations, and multiple spreading of the drop-shaped thickenings over the thin jets.

At $\theta = 30°$ the continuous liquid film covers the cylinder completely after 1 s. Based on this, the average velocity of the film spreading is 0.09 m/s. The local liquid velocity has a maximal absolute value in drop-shaped thickenings on the jets and exceeds the local velocity in the continuous film in about 3.5 times. In the process of liquid flow disturbances occur in the film. Unlike the flow at Re=50 and θ=10°, these disturbances do not propagate upstream and keep their location on the cylinder.

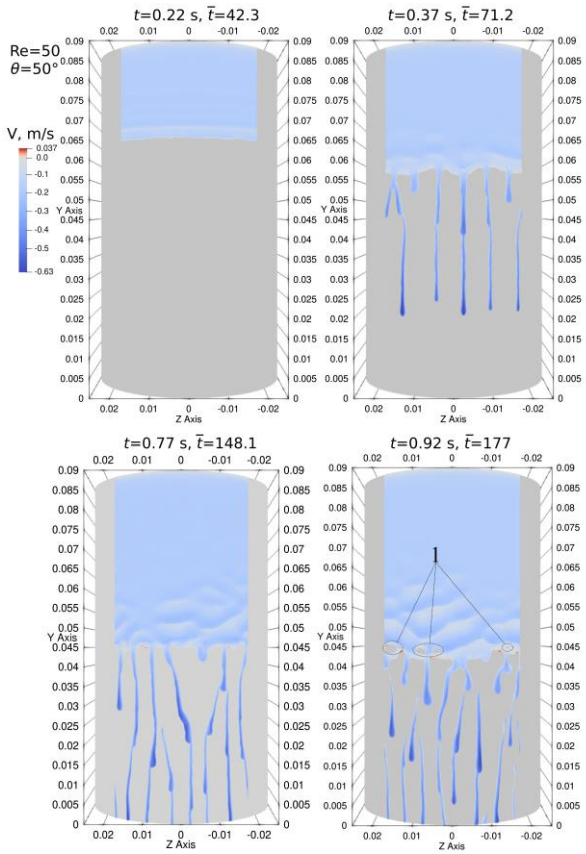

Fig. 6. Fields of the vertical velocity of the liquid (α=0.5) in the refrigerant film flow over the vertical cylinder at $\theta = 50°$. 1 – dry spots.

Figure 6 shows the film spreading of the refrigerant's mixture over the vertical cylinder at $\theta = 50°$. Irregularities occur on the wetting front at $t = 0.22$ s and at a distance of 23 mm from the upper boundary of the cylinder. Further, thin jets with the drop-shaped wetting front form the cascade flow mode. The second generation occurs at $t = 0.37$ s that consists of two jets. The spreading of drop-shaped thickenings takes place over the existed jet tracks similar to the flow at $\theta = 30°$. The wetting front of the continuous film at $\theta = 50°$ falls rather slowly, reaching the extremely low level of $y = 45$ mm at $t = 0.77$ s. Further, dry spots occur in the continuous film near the contact line. Then the continuous film wets the surface again, and the process returns. Such behaviour of the continuous liquid film transforms the flow mode to the jet-droplet one at $t > 0.92$ s.

The average velocity of the continuous film at $\theta = 50°$ tends to zero due to the incomplete wetting of the cylinder. At that, the local liquid velocity has a maximal

absolute value in jets and droplets and exceeds 3 times the local velocity in the continuous film. Some small regions occur on the wetting front of the continuous film and at formation of dry spots, where the liquid flows upstream with the velocity less than 0.037 m/s. The disturbances of the continuous film occurred at $t = 0.37$ s do not propagate upstream.

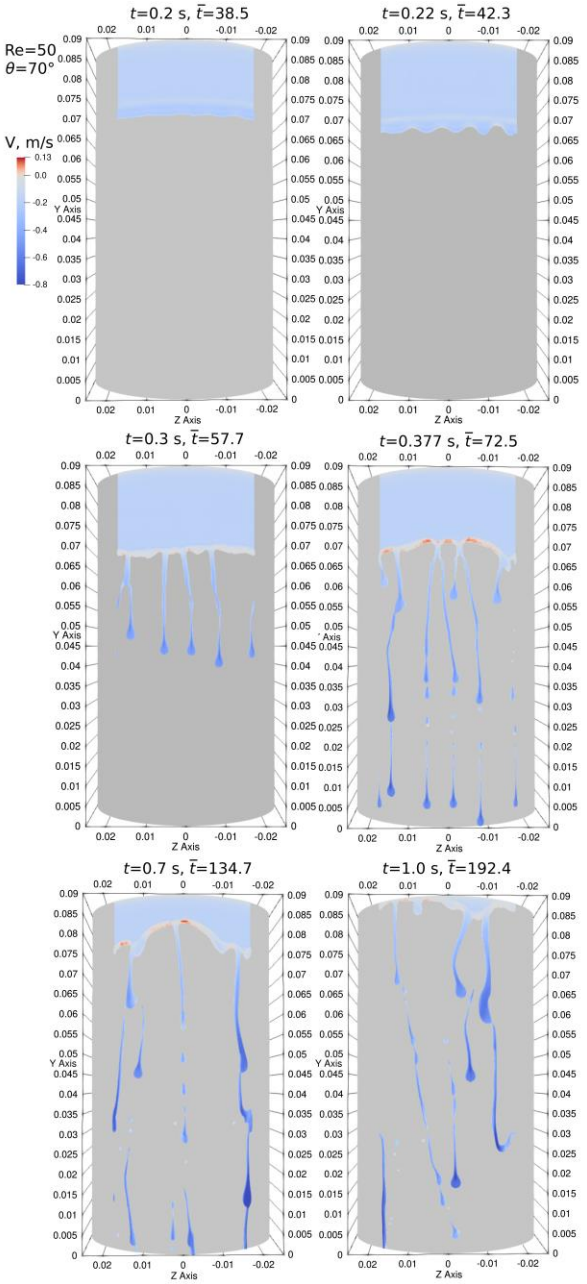

Fig. 7. Fields of the vertical velocity of the liquid (α=0.5) in the refrigerant film flow over the vertical cylinder at $\theta = 70°$.

Figure 7 illustrates the film spreading of the refrigerant mixture over the vertical cylinder at $\theta = 70°$. Irregularities occur on the wetting front at $t = 0.2$ s and at a distance of 17 mm from the upper boundary of the cylinder. The continuous film falls in the maximal distance of 30 mm from the upper boundary of the cylinder at $t = 0.22$ s. The wetting front stays on this distance before $t = 0.3$ s, and the deformed jets with the drop-shaped wetting front develop below it. The second jets generation occurs between first jets at the wetting front of the continuous film at $t = 0.3$ s. At the same time, the wetting front of the continuous film begins its backtrack upon the cylinder, that leads to the jet-droplet liquid flow mode ($t = 0.377$ s and $t = 0.7$ s). At $t = 1$ s, the wetting front reaches practically the initial upper boundary of the cylinder, and the continuous film does not cover the cylinder anywhere.

The maximal absolute value of the local liquid velocity takes place in jets and droplets as well as in the flow cases considered above. This value exceeds 8 times the local liquid velocity in the continuous film. There is the upstream flow of the liquid with the velocity of 0.13 m/s near the sources of the jets from the continuous film. It is worth noting that the disturbances of the continuous film mentioned above (Figure 5 and 6) do not exist in this flow case.

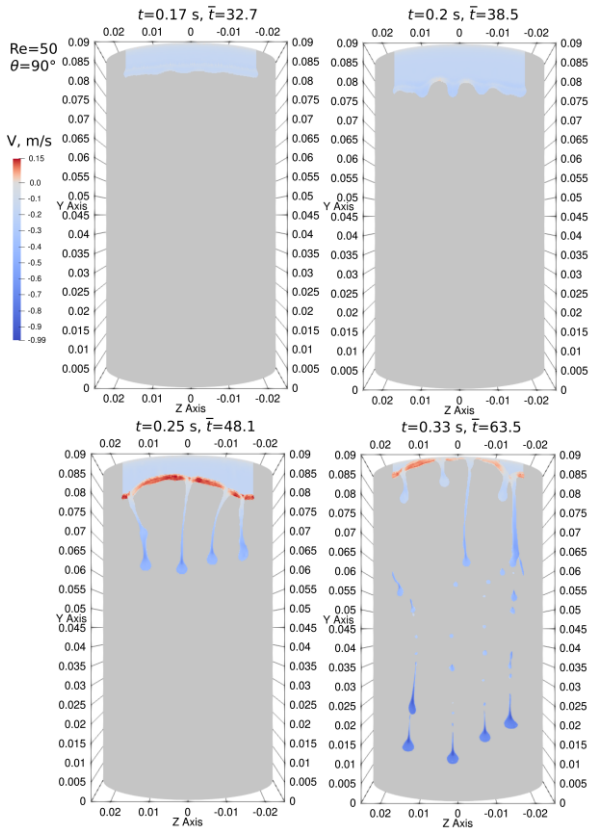

Fig. 8. Fields of the vertical velocity of the liquid (α=0.5) in the refrigerant film flow over the vertical cylinder at $\theta = 70°$.

Figure 8 demonstrates the evolution of the liquid film spreading over the vertical cylinder at $\theta = 90°$. Irregularities occur on the wetting front rather early at $t = 0.17$ s and at a distance of 5 mm from the upper boundary of the cylinder. The wetting front reaches the cylinder height of $y = 0.08$ m at $t = 0.2$ s and does not spread below due to the occurrence of the jets. These jets induce a fast backtrack movement of the contact line between the jets ($t = 0.25$ s), break away from the continuous film and disintegrate on the separate droplets ($t = 0.33$ s). The wetting front reaches the initial upper boundary at $t = 0.33$ s, and the continuous liquid film does not cover the cylinder anywhere. Further, the liquid flows immediately from the upper boundary in the form of separate jets and droplets.

The maximal absolute value of the local velocity $|V|$ = 0.99 m/s takes place in droplets and jets separated from the continuous liquid film. This value is the highest velocity among all flows considered in the paper. The liquid flowing upstream takes place along the whole wetted front (t = 0.25 s) and has a rather high velocity of V = 0.15 m/s. This velocity decreases with the disintegration of the continuous film. There are no any disturbances of the continuous liquid film at θ = 90°.

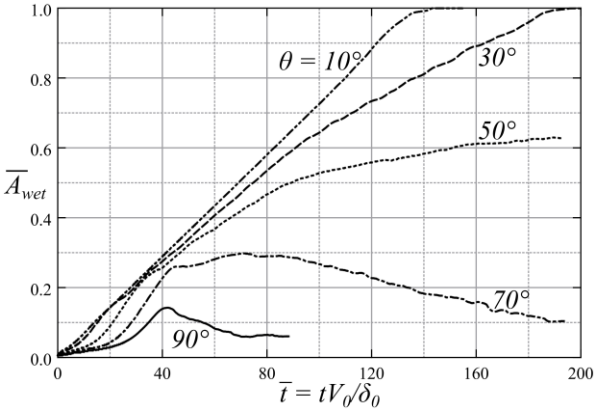

Fig. 9. Dimensionless wetted area at the spreading of refrigerant mixture over the vertical cylinder at Re = 50.

Figure 9 presents dependencies of the cylinder wetted area on time in dimensionless coordinates for all contact angles considered in the paper. The dimensionless area was defined as a ratio of the cylinder wetted area to the quarter of the cylinder sidewall. The dimensionless time was calculated through the initial liquid velocity and film thickness $\bar{t} = t\,|V_0|/\delta$. The wetted area takes into account all regions of the contact between the liquid and the cylinder including droplets and different jets.

At the considered value of Reynolds number, an increase of the contact angle leads to the deceleration of the wetting process up to θ = 50°, when the wetted area leads its limit value of about 63%. Further increase of the contact angle decreases the initially wetted area up to the full disappearance of the continuous film at θ = 90°.

4 Conclusions

Applying VOF-method we performed 3D numerical modeling of R21 (mol. fraction: 0.9) and R114 refrigerant mixture film spreading over the vertical cylinder under isothermal conditions at contact angles from 10° to 90° with the step of 20° and Reynolds number of 50. The investigation has the following results:

– The liquid flows over the cylinder as the continuous film on the initial stage of all considered flow-cases. The drop-shaped irregularities occur on the wetting front after t = 0.16 – 0.23 s. Further flow evolution depends on the contact angle.

– The increase of the contact angle leads to the generation of jets from the irregularities on the wetting front. The jets in flows with contact angles of 10° and 30° have the sharp wetting front.

– The film flow modes change in the following order with increase of the contact angle: the stable jet mode, the cascade jet mode, the jet-droplet mode and the drying mode, when the wetting front of the continuous film passing earlier a certain distance moves back to the initial upper boundary of the cylinder. The stable jet mode has straight or slightly deformed jets, which sources keep their location on the wetting front of the continuous film. Further, liquid spreading over the cylinder takes place in the form of the droplets and jets separated from the continuous film. The jets in the cascade mode occurs periodically on the wetting front of the continuous film between the jet sources of the previous generations. At that, the jets may recombine with each other, and their sources move over the wetting front of the continuous film.

– The backflow of the liquid occurs on the wetting front in the process of drying of the cylinder at the contact angles of 70° and 90°. The velocity of this flow is close to the local velocity of the continuous film on absolute values.

Generally, the contact angle has a key effect on the wetted area due to the change of the liquid spreading modes over the vertical cylinder. These modes are similar ones of flows over the horizontal tubes [2].

This work in the part of liquid film flow simulation was supported by a mega-grant from the Ministry of Science and Higher Education of the Russian Federation (agreement number No. 075-15-2021-575). Also, this research in the part of fluid properties calculation was carried out at the Kutateladze Institute of Thermophysics SB RAS with the financial support from the state contract with IT SB RAS.

References

1. Z. Dai, Y. Zhang, S. Wang, K. Nawaz, A. Jacobi, Int. J. Heat and Mass Transf. **185**, 122407 (2022)
2. X. Hu, A.M. Jacobi, Trans. ASME: J. Heat Transfer **118**, 616 (1996)
3. M. Li, Y. Lu, S. Zhang, Y. Xiao, Desalination **383**, 68 (2016)
4. A. Karmakar, S. Acharya, Int. J. Heat Mass Transf. **173**, 121175 (2021)
5. Z. Ramadan and C.W. Park, Case Studies in Thermal Engin. **24**, 10082 (2021)
6. P. F. de Arroiabe, A. Martinez-Urrutia, X. Peña, M. Martinez-Agirre, M. Mounir Bou-Ali, Int. J. Refrigeration **90**, 12 (2018)
7. Y. Iso, X. Chen, J. Fluids Engin. **133**, 091101 (2011)
8. D. Sebastia-Saez, S. Gu, P. Ranganathan, K. Papadikis, Int. J. Greenhouse Gas Control **19**, 492 (2013)
9. D. Sebastia-Saez, S. Gu, P. Ranganathan, K. Papadikis, Int. J. Greenhouse Gas Control **42**, 388 (2015)
10. D. Sebastia-Saez, S. Gu, M. Ramaioli, Chem. Eng. Sci. **176**, 356 (2018)
11. G. Lavalle, J. Sebilleau, and D. Legendre, Phys. Rev. Fluids **5**, 124001 (2020)

12. H. Ishikawa, S. Ookawara, S. Yoshikawa, Chem. Eng. Sci. **149**, 104 (2016)
13. Y. Haroun, L. Raynal, P. Alix, Chem. Eng. Res. Des. **92**, 2247 (2014)
14. C. Gu, R. Zhang, X. Zhi, S. Zhu, L. Qiu, Cryogenics **110**, 103140 (2020)
15. L.B. Smolka and M. SeGall, Phys. Fluids **23**, 092103 (2011).
16. L.C. Mayo, S.W. McCue, T.J. Moroney, Phys. Rev. E **87** 053018 (2013)
17. C. Ma, W. Wang, M. Shao, Z. Guo, Progr. Comp. Fluid Dyn. **21(3)**, 161 (2021)
18. H. Li, F. Yi, X. Li, A.N. Pavlenko, X. Gao, J. Eng. Thermophysics **27 (1)**, 1 (2018)
19. A.N. Pavlenko, O.A. Volodin, A.S. Surtaev, App. Therm. Engin. **114**, 1265 (2017)
20. A.N. Pavlenko, N.I. Pecherkin, V. E. Zhukov, G. Meski, P. Houghton, Renewable and Sustainable Energy Rev. **132**, 110092 (2020)
21. C.W. Hirt, B.D. Nichols, J. Comp. Phys. **39(1)**, 201 (1981)